SPACE WEATHER, VOL. 6, S10002, doi:10.1029/2007SW000374, 2008

Solar wind drivers of large geomagnetically induced currents during the solar cycle 23

K. E. J. Huttunen,[1] S. P. Kilpua,[1] A. Pulkkinen,[2] A. Viljanen,[3] and E. Tanskanen[4,3]

Received 26 October 2007; revised 19 June 2008; accepted 20 June 2008; published 23 October 2008.

[1] In this paper we investigate the interplanetary drivers of the largest geomagnetically induced currents (GIC) during the solar cycle 23. Interplanetary coronal mass ejections (ICMEs) are the major causes of intense geomagnetic storms and large GIC. In particular, in this work we examine the effectiveness of different structures embedded in an ICME (namely sheath regions, ejecta, and boundary layers) in causing large GIC. It was found that when an ICME interacts with the Earth's magnetosphere the most intense GIC activity is likely to take place during the passage of the turbulent sheath region. The effectiveness of sheath regions in driving large GIC is possibly due to their capability to trigger substorms and to drive intense directly driven ionospheric activity. We also investigated the relationships between different solar wind parameters and the GIC amplitudes. The best correlation with the GIC amplitudes was found with the solar wind electric field and the epsilon parameter. Ejecta-associated GIC seem to require an on-going magnetospheric *Dst* storm while sheath regions and boundary layers can cause large GIC even when no activity is taking place in terms of *Dst*. Interestingly, four of the nine ejecta-associated GIC took place during the recovery phases of a intense magnetic storm (but when *Dst* still was having storm time values below −50 nT).

Citation: Huttunen, K. E. J., S. P. Kilpua, A. Pulkkinen, A. Viljanen, and E. Tanskanen (2008), Solar wind drivers of large geomagnetically induced currents during the solar cycle 23, *Space Weather*, *6*, S10002, doi:10.1029/2007SW000374.

1. Introduction

[2] Rapid temporal changes of the geomagnetic field produce geomagnetically induced currents (GIC) in technological conductor systems such as power grids or pipelines [e.g., *Boteler*, 2003; *Pirjola*, 2000]. As indicated by Faraday's law of induction, the key quantity is the time derivative of the ground magnetic field ($d\mathbf{B}/dt$), which is a reasonable proxy for the GIC activity [*Viljanen et al.*, 2001]. *Pulkkinen et al.* [2006a] showed that the spatiotemporal behavior of $d\mathbf{B}/dt$ above temporal scales of 100 s resembles that of uncorrelated white noise. This sets constraints on the achievable forecasting accuracy of $d\mathbf{B}/dt$ and GIC. So instead of trying to forecast the exact spatiotemporal details of the ground magnetic field and its time derivative [e.g., *Weigel et al.*, 2003], finding statistical relationships between GIC and appropriate geomagnetic parameters may provide a more feasible alternative approach [*Pulkkinen et al.*, 2006b].

[3] For predictive purposes it is important to distinguish between different types of solar wind drivers of large GIC. Significant differences in the magnetospheric response between different types of interplanetary structures have been reported [e.g., *Huttunen et al.*, 2002; *Miyoshi and Kataoka*, 2005] and therefore the GIC response is also expected to be different. *Kataoka and Pulkkinen* [2007] studied GIC activity during intense magnetic storms associated with the interplanetary counterparts of coronal mass ejections (ICMEs) and corotating interaction regions (CIRs) to show partially different physical mechanisms drive GIC during these structures. *Borovsky and Denton* [2006] listed 21 differences between CME-driven and CIR-driven geomagnetic storms. Concerning GIC, in agreement with *Kataoka and Pulkkinen* [2007], they found that CME-driven storms pose most of the problems for ground-based conductor systems, whereas the effect by CIR-driven storms is minor. We will deepen this investigation in this paper by a detailed analysis of the largest GIC storms during the solar cycle 23.

[1]Space Sciences Laboratory, University of California Berkeley, Berkeley, California, USA.
[2]Goddard Earth Sciences and Technology Center, NASA, Greenbelt, Maryland, USA.
[3]Finnish Meteorological Institute, Helsinki, Finland.
[4]Department of Physics and Technology, University of Bergen, Bergen, Norway.

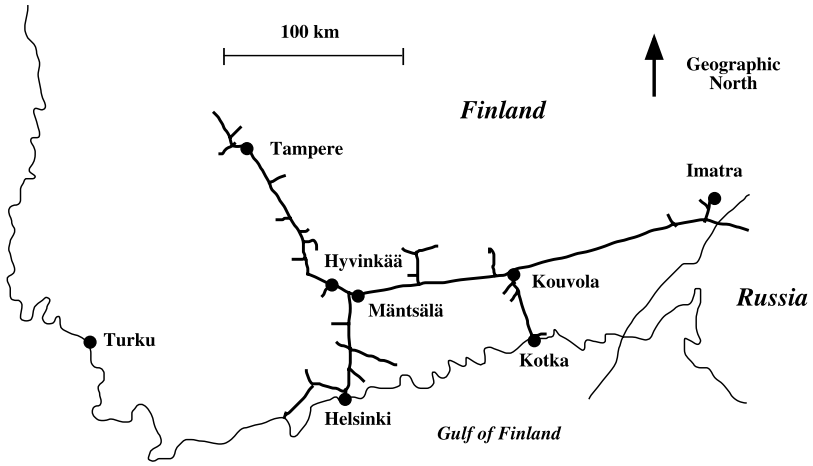

Figure 1. Finnish natural gas pipeline (adapted from *Pulkkinen et al.* [2001]).

[4] ICME itself consists of the following two principal regions that both can drive strong magnetospheric activity [e.g., *Tsurutani et al.*, 1988; *Huttunen and Koskinen*, 2004]: (1) ejecta consisting of the plasma and magnetic field from the CME eruption and (2) sheath of compressed and heated solar wind plasma ahead of the ejecta. It is interesting to separate magnetospheric activity due to sheath and ejecta since the solar wind parameters that control solar wind-magnetospheric coupling have a significantly different behavior during these structures. Within a sheath the dynamic pressure is typically high and variable and the magnetic field direction can change several times from south to north while during an ejecta the magnetic field direction typically changes smoothly over timescales of a day.

[5] In addition to sheath and ejecta, front and tail "boundary layers" can be separated in an ICME. *Wei et al.* [2003] defined the boundary layer as a disturbance structure located between the ejecta and the ambient solar wind characterized by the intensity drop and large directional changes in the magnetic field and the increase in plasma parameters. *Zuo et al.* [2007] pointed out that the magnetic field Z component (B_Z) has more turbulent structure inside boundary layers than inside sheath regions and ejecta making boundary layers good candidates for triggering substorms, which are a major cause of GIC [*Viljanen et al.*, 2006b], and generating high directly driven activity in the ionosphere.

[6] In this paper we investigate solar wind drivers of the largest GIC during solar cycle 23. GIC during intense CIR and ICME storms have been investigated by *Kataoka and Pulkkinen* [2007] and it was found that large GIC events tend to be associated with ICMEs. The purpose of this paper is in particular to investigate what parts of an ICME are responsible for the largest GIC. In section 2 we describe the data sets used and the method of the analysis. Section 3 provides statistical correlations between GIC amplitudes and various solar wind parameters as well as geomagnetic indices. In section 4 we discuss and summarize the results.

2. Used Data and Categorization of Interplanetary Drivers

[7] Solar wind plasma and magnetic field data used in this work were recorded by the ACE satellite that is located near the L1 point more than 200 R_E upstream from the Earth. Plasma measurements by the ACE/SWEPAM instrument are reported with a 64 s time cadence and they were interpolated to the time resolution of the Magnetic Field Experiment (16 s). For three events (15 July 2000, 25 September, and 24 November 2001) that lacked ACE plasma measurements, 1-h averages from the OMNI database were used. Solar wind velocity measurements for the Halloween storm event of 29–31 October 2003 are a product of special ACE/SWEPAM data processing carried out by *Skoug et al.* [2004].

[8] In section 3 we will correlate different solar wind parameters with the GIC amplitudes using a 1.5-h time window [$t_{GIC} - \Delta t_{conv} - 1.5$ h, $t_{GIC} - \Delta t_{conv}$]. The time of the maximum GIC is t_{GIC} and the end time of the window is defined by $t_{GIC} - \Delta t_{conv}$, where the convection time, Δt_{conv}, from the location of ACE (or the spacecraft given in the OMNI database) to the magnetopause has been approximated using the maximum solar wind speed during each event. We also tried different time periods (3, 6, and 12 h), but found the best correlations using the 1.5-h time window for all investigated solar wind parameters.

[9] GIC measurements have been carried out in the Finnish natural gas pipeline (Figure 1) at the Mäntsälä compressor station since November 1998. The Finnish natural gas pipeline is located in southern Finland between magnetic latitudes of about 56°–58°N. The geomagnetic latitude of Mäntsälä is about 57°. The total length of the system in Finland is about 1000 km, but it is connected to the Russian pipeline network of thousands

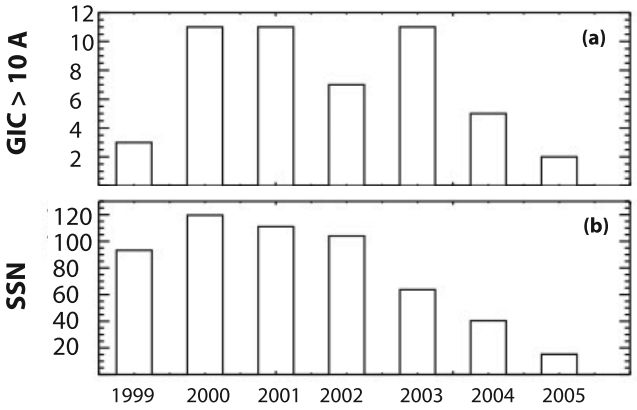

Figure 2. Histograms show (a) the yearly distribution of days with large GIC (maximum amplitude >10 A) and (b) the yearly sunspot number for the solar cycle 23.

of km. However, currents induced in the pipeline in Russia do not practically reach Finland [*Pulkkinen et al.*, 2001]. The measurement technique is described by *Pulkkinen et al.* [2001], and an overview of the results is given by *Viljanen et al.* [2006a]. The temporal resolution of the data is 10 s.

[10] The starting point of the analysis was a list of days during which the maximum GIC exceeded 10 A. Between November 1998 and December 2005 there were 60 such days. The yearly distribution of GIC >10 A days and the yearly sunspot number are shown in Figure 2. The number of days with large GIC was highest at the solar maximum years in 2000–2001 and during the descending phase in 2003 when the "Halloween storms" of 29–31 October 2003 produced the largest GIC of solar cycle 23 [*Pulkkinen et al.*, 2005].

[11] GIC measurements at the Mäntsälä station are unique and as a consequence we are unfortunately constrained to use the data from a single ground station only. Different solar wind parameters are likely biased in importance in generating ionospheric disturbances in different local time (LT) time sectors. The amplitudes of GIC are consequently affected by the LT of the measurement station as it rotates under the influence different ionospheric current systems. It has been shown that the largest GIC are observed at the Mäntsälä station during the local midnight around 2000–0400 LT [*Pulkkinen et al.*, 2003; *Pulkkinen and Kataoka*, 2006]. Because of the LT dependence of GIC we have selected in this study only the GIC events that occurred during near the local midnight of the Mäntsälä station (2000–0400 LT). This should ensure that only the statistically most important class of ionospheric drivers of large GIC are considered in the analysis.

[12] A few large storms are excluded because of missing GIC data in 2004–2005. However, our model calculations, based on the method by *Pulkkinen et al.* [2001], indicate that the maximum GIC during them was less than about 20 A. In 2006, there was only one large storm with the maximum GIC of 14 A, which is not considered here. Before the GIC measurements started, there were a few large magnetic storms in the beginning of solar cycle 23 in 1996–1998, which could have caused GIC larger than 10 A.

[13] We have divided GIC drivers into the following three principal categories: (1) ICME, (2) CIR, and (3) shock related. In addition, the ICME related GIC events are divided into three subcategories that are marked as follows in Figure 3: 1A, sheath; 1B, boundary layer (BL); and 1C, ejecta. Following the study by *Wei et al.* [2003] we chose the length of the front boundary layer (FBL) to be 1.7 h and the length of the end boundary layer (EBL) to be 3.1 h. Note that if the same structure caused GIC values >10 A in two consequent days the smaller GIC event has been excluded from the study.

[14] The ICME event on 30–31 October 2003 presented in Figure 3 demonstrates that all different parts of an ICME separated in this work can drive large GICs during a single ICME. In addition to the daily GIC maximum (if >10 A) we also included in the analysis the GIC maximum of each substructure of the ICME if it was larger than 10 A. In total, the analysis included 35 GIC events with current peak GIC amplitude larger than 10 A. The largest GIC with the amplitude of 57.0 A recorded during the investigated period occurred on 29 October 2003 during a sheath region. However this GIC took place when the Mäntsälä station was in the noon sector and it was excluded from the study.

3. Results

[15] The summary of the GIC activity depending on the solar wind driver is listed in Table 1. Statistics show that the majority (91%) of the large GIC events were associated with the ICMEs whereas CIRs caused only two large GIC during the 7-year period investigated. In addition, there was one shock associated large GIC event. The most effective substructure of an ICME in causing large GIC is a sheath region: sheath regions were responsible for the largest number of GIC >10 A events and they were associated with the highest average of the maximum |GIC|, which is 24.2 A. In addition, sheath regions caused more than half of the 10 largest GIC events (the N_{10} row in Table 1). Ejecta was found to be the least efficient part of an ICME in driving significant GIC activity.

[16] In the following we will compare the maximum GIC amplitudes with the maximum values of the selected solar wind parameters (determined during the 1.5-h time window before the maximum |GIC|) whose variations are known to cause rapid enhancements of ionospheric and magnetospheric current systems. Figure 4 gives the scatterplots of $|\mathrm{GIC}|_{\max}$ as a function of the maximum values of the GSM Y component of the solar wind electric field $|E_Y|_{\max}$ (Figure 4a), the time derivative of the IMF Z component $|dB_Z/dt|_{\max}$ (Figure 4b), in nT/s, and the solar wind dynamic pressure $(P_{\mathrm{dyn}})_{\max}$ (Figure 4c). $|dB_Z/dt|$ was calculated using the sampling frequency of the magnetic field, 16s.

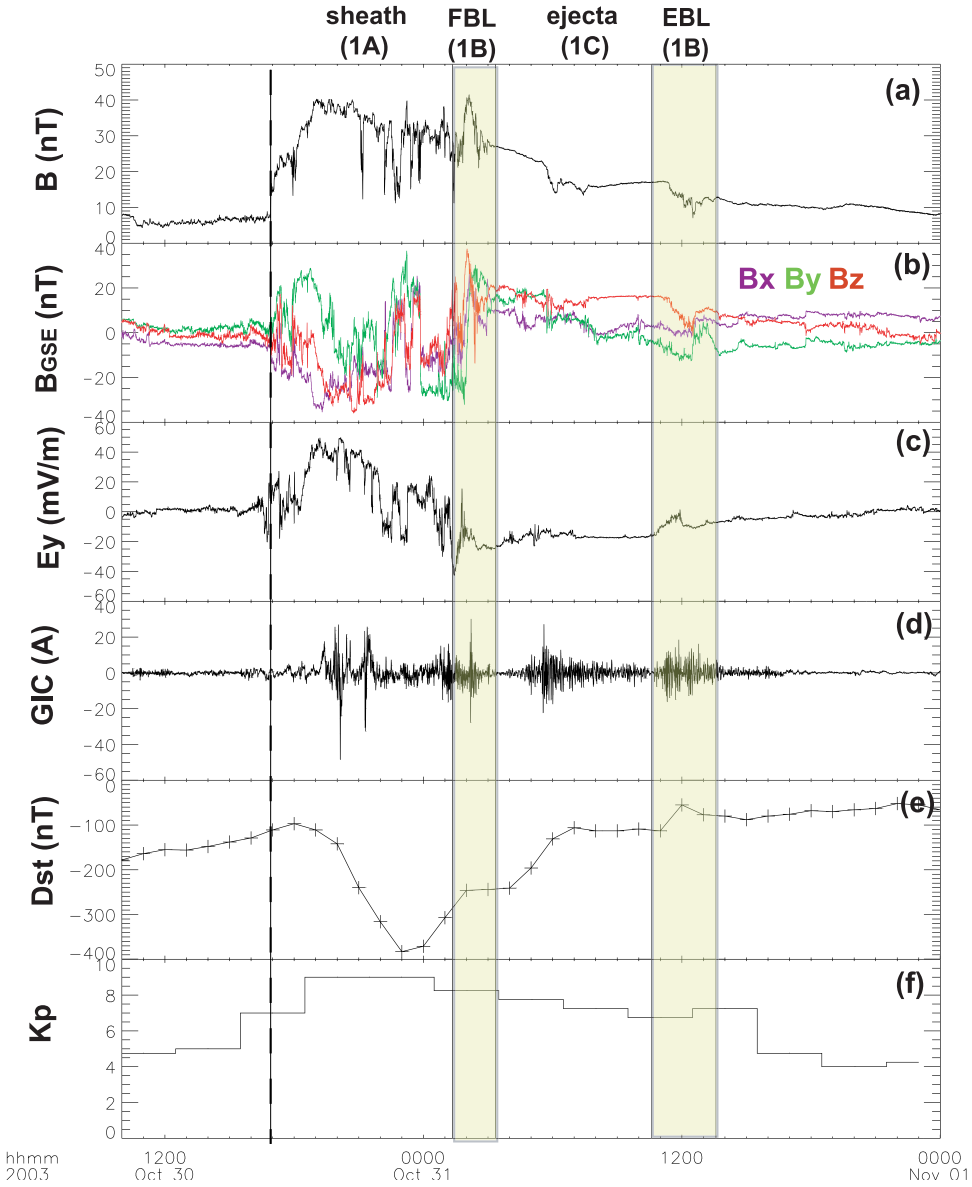

Figure 3. ACE measurements during an ICME on October 2003. Different regions of the ICME are indicated in the plot. (a) Magnetic field magnitude, (b) magnetic field components in GSM coordinates, (c) *Y* component of the solar wind electric field, (d) GIC amplitude recorded from the Finnish natural gas pipeline at Mäntsälä, and (e) *Dst* and (f) *Kp* indices are shown. The dashed line indicates the time of the shock and the yellow regions define the front boundary layer (FBL) and the end boundary layer (EBL) boundary.

[17] Figures 4d–4f examine the strength and duration of the energy loading from the solar wind to the magnetosphere prior to the investigated maximum |GIC|. The energy input is estimated using the Akasofu epsilon parameter ($\epsilon = 10^7\ VB^2 l_0^2 \sin^4(\theta/2)$, using SI units) that is given in terms of the solar wind speed V and IMF magnitude B and the direction $\tan\theta = B_Y/B_Z$ [see *Akasofu*, 1979]. l_o is an empirical parameter to fit the average energy input to the average estimated output. Maximum values of the epsilon parameter ϵ_{max} are given in Figure 3d and the integrated epsilon parameter (over the 1.5-h time window) is given in Figure 3e. Finally, the total time when the IMF was significantly southward (defined by $B_Z < -10$ nT) during the 1.5-h time window is displayed in Figure 4f.

[18] Visual inspection of Figure 4 shows that in general the larger values the investigated solar wind parameters have larger associated GIC, but there are considerable

Table 1. Statistics of the 60 Large Amplitude GIC Events During the Solar Cycle 23[a]

	Sheath	Ejecta	BL	CIR	Shock
N	13	9	10	2	1
$\langle \lvert GIC \rvert_{max} \rangle$ (A)	24.2	17.5	22.4	19.8	11.4
N_{10}	5	1	4	0	0
$\langle \lvert E_Y \rvert_{max} \rangle$ (mV/m)	19.3	17.8	24.1	7.2	
$\langle \lvert dB_Z/dt \rvert_{max} \rangle$ (nT/s)	0.80	0.37	0.82	0.38	
$\langle (P_{dyn})_{max} \rangle$ (nPa)	27.5	12.1	22.5	7.1	
$\langle (\epsilon)_{max} \rangle$ (10^{13} J)	1.4	1.0	1.8	0.19	
$\langle (W_\epsilon)_{max} \rangle$ (10^{16} J)	3.6	3.0	3.4	0.36	

[a]Rows from top to bottom the number of GIC > 10 A in each driver category (N), the averages of the maximum |GIC|, the distributions of the 20 and 10 largest GIC between different driver categories (N_{20} and N_{10}), and the last five rows give the averages of the maximum values of the selected solar wind parameters (see text for details). Only the events that occurred within the local midnight of the Mäntsälä station (2000 – 0400 LT) have been considered in this study.

scatters in the relationships. It is also seen that for sheath and BL categories the range of solar wind parameters is greater than for the ejecta category and it appears that the correlation are somewhat higher. However, since the number of events in each category is low we have only included correlation coefficients for the whole data set. The highest correlation was found between $|GIC|_{max}$ and the maximum values of $|E_Y|$ and the epsilon parameter, with the correlation coefficients of 0.56 and 0.55 respectively. Note that the epsilon parameter and the E_Y are closely related and thus it is expected that these parameters exhibit very similar correlation with $|GIC|_{max}$. The ranges in E_Y ($\max(E_Y) - \min(E_Y)$) correlated also well with the $|GIC|_{max}$, with the correlation coefficient of 0.54 (data not shown). The lowest correlation was found with $|dB_Z/dt|_{max}$ and solar dynamic pressure with the correlation coefficient of 0.30 and 0.40, respectively.

[19] The average energy input to the magnetosphere (integrated epsilon parameter) was about the same for all ICME related categories, but was an order of magnitude smaller for the CIR associated GIC. As a comparison an intense magnetic storm requires the energy input $\sim 10^{16}$ J using the solar wind speed 500 km/s and the criteria by *Gonzalez et al.* [1994] that states that the sufficient condition to generate $Dst < -100$ nT storm is $B_Z < -10$ nT for more than 3 h. Figure 4f shows that the ejecta associated events were either preceded by long periods of the significantly southward IMF ($B_Z < -10$ nT) or with no $B_Z < -10$ nT at all. Sheath and BL associated GIC were associated with wide range of $B_Z < -10$ nT periods.

[20] It is interesting to note that there was a considerable fraction (21% or 7 out of total 34 events presented in Figure 4f) of events for which B_Z was >-10 nT during the whole 3-h period. Four of these events were GIC associated with ejecta and took place in the recovery phase of an intense magnetic storm (see also Figure 5 that shows that all events in category ejecta are associated with *Dst* close to -100 nT or below). The number of ejecta associated GIC with B_Z only weakly southward or northward remained the same even if the length of the window was increased to 3 h.

[21] Correlations between the maximum GIC and the *Dst* and *Kp* indices are plotted in Figures 5a and 5b. Correlation is significantly higher between the GIC amplitude and *Kp* than between the GIC amplitude and *Dst*, with correlation coefficients 0.54 and -0.18 respectively. Only ejecta associated events show a moderate correlation between GIC and *Dst*. In addition, Figure 5 demonstrates that all large GIC values occur during storm time *Kp* values (i.e., $Kp > 5$), but large GIC can occur even when no significant geomagnetic activity is taking place in terms of *Dst*. This is consistent with the result by *Viljanen et al.* [2006a] who found that GIC >10 A have occurred only if the local *K* index exceeds 5.

4. Discussion and Conclusions

[22] In this paper we have studied solar wind drivers of the largest GIC (amplitudes >10 A) at the Mäntsälä station, part of the Finnish pipeline network, during solar cycle 23. Solar wind drivers were divided into shock, ICME and CIR related. ICME associated events were further divided in three subcategories including, sheath, boundary layer (BL) and ejecta. The main purpose of the paper was to investigate the effectiveness of these different parts of ICMEs in causing large GIC.

[23] The amplitude of GIC depends on the local time of the measuring station and statistically the largest GIC occur near the local midnight. To avoid the biasing of the results by this LT dependence we selected in this work only the GIC events that occurred within the local midnight of the the Mäntsälä station (2000 – 0400 LT). Consistent with the previous studies [*Kataoka and Pulkkinen*, 2007], the majority of large GIC were ICME associated (91%) whereas CIRs caused only two GIC > 10 A events during the investigated period. In addition an interplanetary shock caused one large GIC event.

[24] We found that sheath regions are the substructure of an ICME that most likely leads to a large GIC. In our data set of 35 events sheath regions caused most large GIC events with the highest-average amplitudes of all categories. Ejecta are also important causes of large GIC, but the amplitudes were on average lower than the GIC amplitudes associated with sheaths and boundary layers. Furthermore, from the ten largest GIC events of solar cycle 23 only one was caused by an ejecta while sheath regions were responsible for five of these events.

[25] We also investigated the relationships between various solar wind parameters and the GIC amplitudes. In general large GIC take place when solar wind conditions are highly disturbed. The average maximum values of the investigated solar wind parameters were largest for the sheath regions and boundary layers and smallest for the category CIR. The highest correlation was found with the GIC amplitude and the maximum value of the

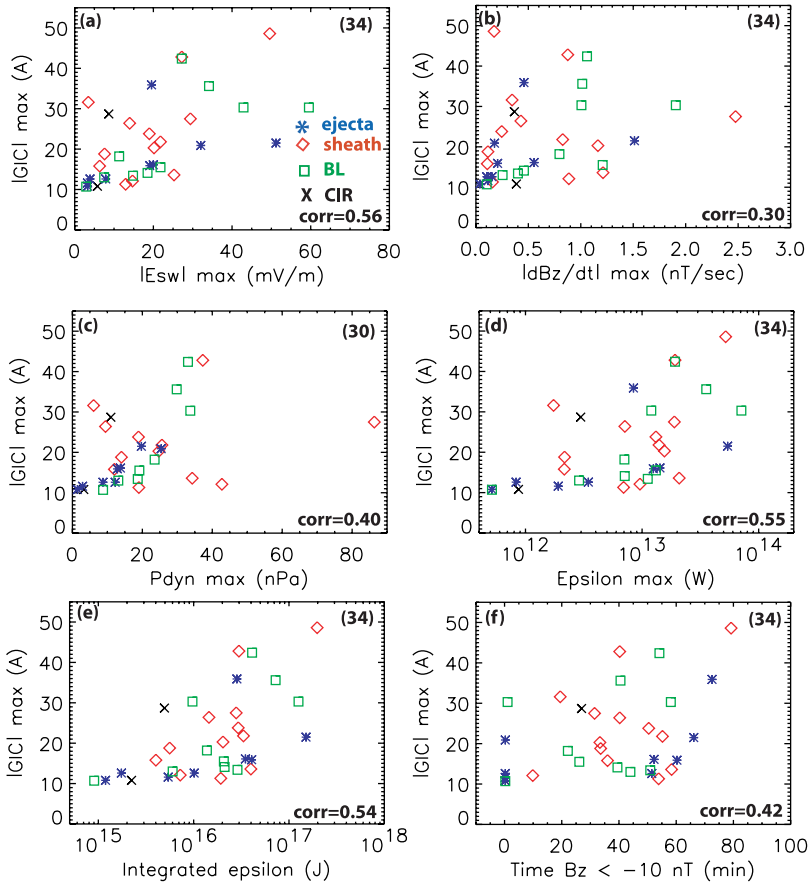

Figure 4. Scatterplots of the max(|GIC|) and the maximum values of (a) the *Y* component of the solar wind electric field, (b) the time derivative of the *Z* component of IMF, (c) the solar wind dynamic pressure, (d) the maximum value of the epsilon parameter, and (e) the integrated epsilon parameter. (f) The total time during the 1.5-h time window before the time of the maximum |GIC| when the IMF *Z* component was <−10 nT. Correlation coefficients are indicated in each figure. Note that in Figures 3d and 3e the correlations are calculated against the epsilon (and not the logarithmic epsilon). The numbers in parenthesis indicate the total number of data points in the scatterplot of that particular figure. The Halloween ICMEs on 29−31 October 2003 that were responsible of four large GICs lacked the solar wind density measurements.

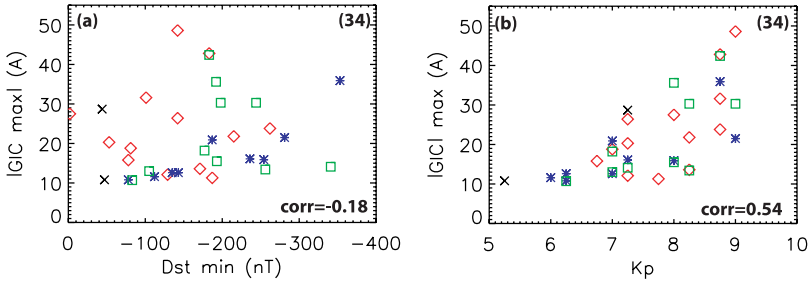

Figure 5. Scatterplot of the maximum |GIC| and (a) the *Dst* index as well as (b) the 3-h *Kp* index at the time of the |GIC| maximum.

solar wind electric field and the maximum value of the epsilon parameter, but in general there were large scatters in the relationships.

[26] From the general space physics viewpoint it is clear that GIC are not a direct consequence of the solar wind fluctuations but rather a result of a complex chain of interactions in the solar wind- magnetosphere-ionosphere system. As dynamics of each individual subcomponent in this system is also complex, it is reasonable to expect that despite the existing physical link there will be large scatter, for example, in a GIC response to given solar wind electric field magnitudes.

[27] When calculating correlations we tried different time windows (from 1.5 to 12 h) and the correlations were found to be highest for the shortest time window implying relatively small time lag between the solar wind perturbation arriving at the magnetopause and the large GIC. The energy input from the solar wind to the magnetosphere was estimated using the epsilon parameter. We found a moderate positive correlation between the integrated epsilon parameter and GIC amplitudes and that the intense energy loading preceded most of the investigated events. It was found that in general ejecta were associated with the longest periods of significantly southward magnetic field while sheath and boundary layers were associated with greater range of the energy input. However, the analysis revealed that intense GIC also take place when the energy loading is weak and the IMF is not significantly southward. The majority of these events were ejecta associated that occurred in the recovery phases of intense magnetic storms.

[28] The differences between the GIC events caused by different substructures of an ICME reflect the different behavior of the magnetic field and plasma parameters in these structures. Auroral substorms are considered as one of the major causes of large GIC and because of the smoothly varying magnetic field direction and the low variance in solar wind parameters ejecta lack external triggering of substorms and rapid directly driven enhancements of auroral electrojets [*Tsurutani et al.*, 2004]. Ejecta are rather associated with the relatively continuous dissipation of solar wind energy. On the contrary sheath regions and boundary layers are associated with large and rapid changes in the magnetic field direction and pressure pulses that effectively trigger substorm expansion phases and that can drive in general intense ionospheric disturbances. It was also found by *Huttunen et al.* [2002] that sheath regions are likely to generate more intense *Kp* response than ejecta.

[29] Ejecta associated GIC seem to require an on-going *Dst* storm (either main phase or recovery phase) and we found a moderate positive correlation between *Dst* and the maximum GIC whereas sheath and boundary layers can cause large GIC even if no significant geomagnetic activity is taking place in terms of *Dst*. The largest GIC of the solar cycle 23 (57.0 A on 29 October 2003) took place when *Dst* was barely at the intense storm level while the largest *Dst* storm of the solar cycle 23 (on 20 November 2003 with *Dst* minimum of −422 nT) was associated with much lower-amplitude GIC (23.8 A).

[30] From the predictive point of view it is interesting to find differences between the GIC activity caused by the different substructures of an ICME. The results of this work suggest that when an ICME hits the Earth, largest GIC are expected relatively shortly after the shock arrival when the Earth's magnetosphere interacts with the turbulent sheath region preceding the ejecta. While the positive correlations between the solar wind electric field and the epsilon parameter was established more quantitative analysis is needed. An important outstanding question that will be a subject of further study is that do large solar wind convective electric fields lead always to large GIC?

[31] **Acknowledgments.** We wish to thank the Gasum Oy company for a long-term collaboration in GIC studies of the Finnish natural gas pipeline network. R. Skoug is acknowledged for providing the ACE/SWEPAM data for the Halloween storm event. We thank N. Ness for the ACE magnetic field data and D. J. McComas for the ACE solar wind data. These data were obtained through the Coordinated Data Analysis Web (CDAWeb). The *Dst* and *Kp* values were obtained from the World Data Center C2 in Kyoto. The yearly sunspot number were obtained RWC Belgium World Data Center for the Sunspot Index.

References

Akasofu, S.-I. (1979), Interplanetary energy flux associated with magnetospheric substorms, *Planet. Space Sci.*, *27*, 425–431.

Borovsky, J. E., and M. H. Denton (2006), Differences between CME-driven storms and CIR-driven storms, *J. Geophys. Res.*, *111*, A07S08, doi:10.1029/2005JA011447.

Boteler, D. H. (2003), Geomagnetic hazards to conducting networks, *Natural Hazards*, *28*, 537–561.

Gonzalez, W. D., J. A. Joselyn, Y. Kamide, H. W. Kroehl, G. Rostoker, B. T. Tsurutani, and V. M. Vasyliunas (1994), What is a geomagnetic storm?, *J. Geophys. Res.*, *99*(A4), 5771–5792.

Huttunen, K. E. J., and H. E. J. Koskinen (2004), Importance of post-shock streams and sheath region as drivers of intense magnetospheric storms and high-latitude activity, *Ann. Geophys.*, *22*, 1729–1738.

Huttunen, K. E. J., H. E. J. Koskinen, and R. Schwenn (2002), Variability of magnetospheric storms driven by different solar wind perturbations, *J. Geophys. Res.*, *107*(A7), 1121, doi:10.1029/2001JA900171.

Kataoka, R., and A. Pulkkinen (2007), Geomagnetically induced currents during intense storms driven by coronal mass ejections and corotating interacting regions, *J. Geophys. Res.*, *113*, A03S12, doi:10.1029/2007JA012487.

Miyoshi, Y., and R. Kataoka (2005), Ring current ions and radiation belt electrons during geomagnetic storms driven by coronal mass ejections and corotating interaction regions, *Geophys. Res. Lett.*, *32*, L21105, doi:10.1029/2005GL024590.

Pirjola, R. (2000), Geomagnetically induced currents during magnetic storms, *IEEE Trans. Plasma Sci.*, *28*, 1867–1873.

Pulkkinen, A., and R. Kataoka (2006), S-transform view of geomagnetically induced currents during geomagnetic superstorms, *Geophys. Res. Lett.*, *33*, L12108, doi:10.1029/2006GL025822.

Pulkkinen, A., A. Viljanen, K. Pajunpää, and R. Pirjola (2001), Recordings and occurrence of geomagnetically induced currents in the Finnish natural gas pipeline network, *J. Appl. Geophys.*, *48*, 219–231.

Pulkkinen, A., A. Thomson, E. Clarke, and A. McKay (2003), April 2000 geomagnetic storm: Ionospheric drivers of geomagnetically induced currents, *Ann. Geophys.*, *21*, 709–717.

Pulkkinen, A., S. Lindahl, A. Viljanen, and R. Pirjola (2005), Geomagnetic storm of 29–31 October 2003: Geomagnetically induced currents and their relation to problems in the Swedish high-voltage power transmission system, *Space Weather*, *3*, S08C03, doi:10.1029/2004SW000123.

Pulkkinen, A., A. Klimas, D. Vassiliadis, V. Uritsky, and E. Tanskanen (2006a), Spatiotemporal scaling properties of the ground geomagnetic field variations, *J. Geophys. Res.*, *111*, A03305, doi:10.1029/2005JA011294.

Pulkkinen, A., A. Viljanen, and R. Pirjola (2006b), Estimation of geomagnetically induced current levels from different input data, *Space Weather*, *4*, S08005, doi:10.1029/2006SW000229.

Skoug, R. M., J. T. Gosling, J. T. Steinberg, D. J. McComas, C. W. Smith, N. F. Ness, Q. Hu, and L. F. Burlaga (2004), Extremely high speed solar wind: 29–30 October 2003, *J. Geophys. Res.*, *109*, A09102, doi:10.1029/2004JA010494.

Tsurutani, B. T., W. D. Gonzalez, F. Tang, S. I. Akasofu, and E. J. Smith (1988), Origin of interplanetary southward magnetic fields responsible for major magnetic storms near solar maximum (1978–1979), *J. Geophys. Res.*, *93*, 8519–8531.

Tsurutani, B. T., X.-Y. Zhou, and W. D. Gonzalez (2004), A lack of substorm expansion phases during magnetic storms induced by magnetic clouds, in *Disturbances in Geospace: The Storm-Substorm Relationship*, *Geophys. Monogr. Ser.*, vol. *142*, edited by A. S. Sharma, Y. Kamide, and G. S. Lakhina, pp. 23–36, AGU, Washington, D. C.

Viljanen, A., H. Nevanlinna, K. Pajunpää, and A. Pulkkinen (2001), Time derivative of the horizontal geomagnetic field as an activity indicator, *Ann. Geophys.*, *19*, 1107–1118.

Viljanen, A., A. Pulkkinen, R. Pirjola, K. Pajunpää, P. Posio, and A. Koistinen (2006a), Recordings of geomagnetically induced currents and a nowcasting service of the Finnish natural gas pipeline system, *Space Weather*, *4*, S10004, doi:10.1029/2006SW000234.

Viljanen, A., E. I. Tanskanen, and A. Pulkkinen (2006b), Relation between substorm characteristics and rapid temporal variations of the ground magnetic field, *Ann. Geophys.*, *24*, 725–733.

Wei, F., R. Liu, Q. Fan, and X. Feng (2003), Identification of the magnetic cloud boundary layers, *J. Geophys. Res.*, *108*(A6), 1263, doi:10.1029/2002JA009511.

Weigel, R. S., A. J. Klimas, and D. Vassiliadis (2003), Solar wind coupling to and predictability of ground magnetic fields and their time derivatives, *J. Geophys. Res.*, *108*(A7), 1298, doi:10.1029/2002JA009627.

Zuo, P. B., F. S. Wei, X. S. Feng, and F. Yang (2007), The relationship between the magnetic cloud boundary layer and the substorm expansion phase, *Sol. Phys.*, *242*, 167–185.

K. E. J. Huttunen and S. P. Kilpua, Space Sciences Laboratory, University of California Berkeley, 7 Gauss Way, Berkeley, CA 94720-7450, USA. (huttunen@ssl.berkeley.edu; samik@ssl.berkeley.edu)

A. Pulkkinen, Goddard Space Flight Center, NASA, Mail Code 674, Greenbelt, MD 20771, USA. (antti.a.pulkkinen@nasa.gov)

E. I. Tanskanen, Department of Physics and Technology, University of Bergen, Allgaten 55, N-5007 Bergen, Norway. (eija.tanskanen@fmi.fi)

A. Viljanen, Finnish Meteorological Institute, P. O. Box 503, Helsinki, Finland. (ari.viljanen@fmi.fi)